from mixed cell cultures or harvested tissues by using a QIAamp DNA Mini Kit (Qiagen Inc., Valencia, CA). To detect human cells in the mouse tissues, a set of human *Alu* primers (sense: 5′-CTG AGG TCA GGA GTT CGA G-3′; and antisense: 5′-TCA AGC GAT TCT CCT GCC-3′) were designed. We performed the quantitative real-time PCR assay by using a LightCycler instrument (Roche Molecular Biochemicals, Indianapolis, IN). PCR amplification began with a 120-second denaturation step at 95°C and then 30 cycles of denaturation at 95°C for 30 seconds, annealing at 63°C for 30 seconds, and extension at 72°C for 30 seconds. We also amplified the mouse *GAPDH* genomic DNA sequence with mouse *GAPDH* primers (sense: 5′-CCA CTC TTC CAC CTT CGA T-3′; and antisense: 5′-CAC CAC CCT GTT GCT GTA-3′) by using the same PCR conditions described for *Alu*. The amounts of *E1A* DNA of OBP-301 and OBP-401 were measured as previously described. The sequences of specific primers used for *E1A* were as follows: sense: 5′-CCT GTG TCT AGA GAA TGC AA-3′; and antisense: 5′-ACA GCT CAA GTC CAA AGG TT-3′. PCR amplification of genomic DNA extracted from mouse lymph nodes was performed with precycling heat activation of DNA polymerase at 95°C for 600 seconds, followed by 40 cycles of denaturation at 95°C for 10 seconds, annealing at 58°C for 15 seconds, and extension at 72°C for 8 seconds. Data analysis was performed with LightCycler Software (Roche Molecular Biochemicals).

### Statistical Analysis

We used the Student 2-tailed *t* test to identify statistically significant differences between groups. Results are reported as mean ± SEM. *P* values less than 0.05 were considered statistically significant.

## RESULTS

### In Vitro Purging of Human Colorectal Cancer Cells by Telomerase-Specific Oncolytic Adenovirus

To examine whether telomerase-specific oncolytic adenovirus can selectively kill human tumor cells among the millions of lymphocytes in lymph nodes, HT29 human colorectal cancer cells were mixed with PBMC from healthy donors and purged in vitro with OBP-301 for 3 days. Viable HT29 cells were then visualized with GFP fluorescence by OBP-401 infection for 24 hours (see Figure, Supplemental Digital Content 2, online only, available at http://links.lww.com/SLA/A39, which illustrates the procedures for in vitro purging experiments). No GFP-positive viable HT29 cells were detected at 3 days postpurging with OBP-301, whereas infection with replication-deficient control adenovirus dl312 had no significant effects on the viability of HT29 cells (Fig. 1A) (see Figure, Supplemental Digital Content 2, online only, available at: http://links.lww.com/SLA/A39, which demonstrates in vitro purging effect of OBP-301 infection). The purging efficacy of OBP-301 was also confirmed by measuring the relative GFP expression of samples by using a fluorescence microplate reader (Fig. 1B). Neither OBP-301 nor dl312 infection affected the viability of PBMC, confirming the safety of OBP-301 to normal human lymphocytes (Fig. 1C). Next, we determined if human tumor cells mixed with mouse lymphocytes obtained from the spleen would be sensitive to OBP-301 treatment. As expected, purging with OBP-301 significantly reduced the number of viable HT29 cells in mouse splenocytes compared with mock- or dl312-treated samples (Fig. 1D).

### In Vivo Lymphatic Spread of Virus on Regional Lymph Nodes

To verify that oncolytic adenoviruses traffic through the lymphatics to the regional lymph nodes, we used an orthotopic mouse model of human rectal cancer with spontaneous lymph node metastasis. We first determined whether the regional lymphatic system, including lymphatic vessels and lymph nodes, could be assessed by injecting dye into the primary tumors. Intense blue staining was detected in regional lymph nodes as early as 1 minute after injection of indigo carmine blue dye into the primary rectal tumors, indicating that the injected solution could rapidly enter the intratumoral lymphatics, which provides a route from the primary tumor to draining lymph nodes (Fig. 2A). Five days after OBP-401 injection into the primary tumors, we also detected GFP expression in both primary rectal tumors and metastatic lymph nodes under the laparotomy by using a 3-chip CCD optical imaging system (Fig. 2B).

To further evaluate the selective replication ability of telomerase-specific oncolytic adenovirus in metastatic lymph nodes, we measured the relative amounts of *E1A* DNA by quantitative real-time PCR analysis. The metastatic GFP-positive lymph nodes con-

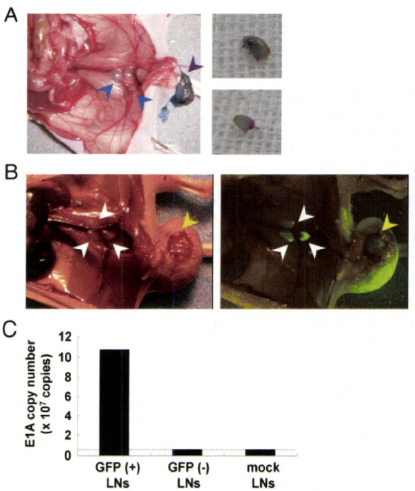


**FIGURE 2.** In vivo lymphatic spread of virus on regional lymph nodes. A, A lymphatic drainage pattern in an orthotopic xenograft of human HT29 cells. The abdominal cavity was photographed 1 minute after injection of 1% indigo carmine blue dye into an established orthotopic HT29 tumor. Arrowheads indicate the lymph nodes stained with blue dye. Gross appearance of the abdominal cavity (left) and excised lymph nodes (right). B, Five days after intratumoral injection of $1 \times 10^8$ PFU of OBP-401, HT29 tumor-bearing *nu/nu* mice were assessed for lymph node metastasis during laparotomy. Macroscopic (left) and fluorescent (right) images. Primary tumor (yellow arrowhead) and metastatic lymph nodes (white arrowheads) are shown. C, Assessment of viral replication in metastatic lymph nodes. GFP-positive and -negative lymph nodes were harvested from mice with HT29 tumor xenografts 5 days after injection of $1 \times 10^8$ PFU of OBP-401 and then subjected to real-time quantitative PCR assay to quantify the amounts of viral *E1A* copy number. The value in mock-infected lymph nodes is indicated with a dotted line as a baseline level.

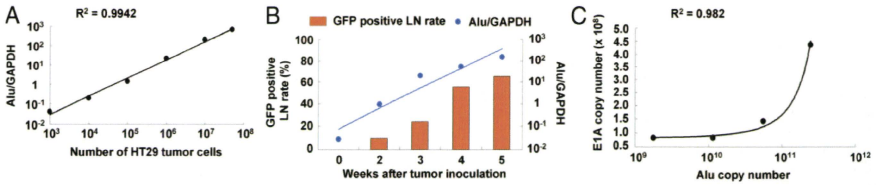


**FIGURE 3.** Detection and quantification of human cancer cells in mouse tissues with a quantitative real-time *Alu*PCR analysis. A, Generation of a standard curve. Mouse splenocytes ($5 \times 10^7$ cells) were spiked with serially diluted HT29 human colorectal cancer cells. Genomic DNA was extracted from the mixtures and then subjected to the quantitative amplification (see Figure, Supplemental Digital Content 4A, available at: http://links.lww.com/SLA/A41, which illustrates schematic procedures of detection and quantification of human cancer cells in mouse splenocytes). The *Alu*/*GAPDH* ratios *versus* the numbers of spiked HT29 cells are presented. Regression analysis yielded a correlation coefficient of $R^2 = 0.9942$. The data are representative of 3 separate experiments. B, Quantitative analysis of spontaneous lymph node metastasis. Genomic DNA was extracted from the lymph nodes of mice bearing human HT29 tumor xenografts at the indicated time points after tumor inoculation and analyzed with the quantitative *Alu*PCR assay (see Figure, Supplemental Digital Content 4B, available at: http://links.lww.com/SLA/A41, which illustrates schematic procedures of detection and quantification of human cancer cells in mouse tissues). Metastatic lymph nodes were simultaneously visualized by injecting $1 \times 10^8$ PFU of OBP-401 into the primary tumors 5 days before lymph node isolation. C, The viral *E1A* copy numbers were also determined in genomic DNA extracted from isolated lymph nodes by the quantitative real-time PCR method and plotted *versus* the *Alu* copy numbers.

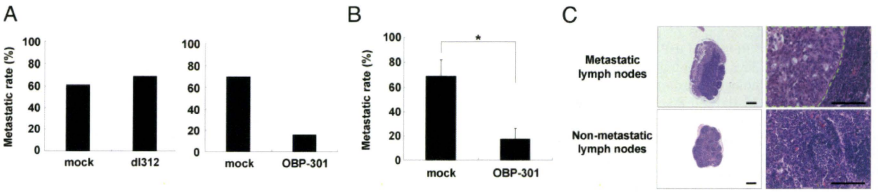


**FIGURE 4.** Histologic evaluation of selective antitumor effect of OBP-301 delivered into primary tumors on lymphatic metastasis in a colorectal cancer xenograft model. Mice bearing orthotopic HT29 tumors received 3 courses of intratumoral injections of $1 \times 10^8$ PFU of OBP-301 or dl312 every 2 days beginning on day 14 after the tumor inoculation. A, On day 35, we harvested a total of 23 to 29 lymph nodes from 5 to 8 mice per group, stained them with hematoxylin and eosin, and calculated metastatic rates. B, In a separate experiment, metastatic rates were histologically determined in individual mice and averaged with S.E.M. ($n = 8$). A single asterisk denotes statistical significance ($P < 0.05$) as compared with the mock group. C, Paraffin-embedded sections of lymph nodes with or without metastatic foci were obtained 35 days after tumor cell implantation and stained with hematoxylin and eosin. Left, ×40 magnification; right, ×200 magnification. Scale bar, 100 μm. The area with metastatic HT29 cells is indicated with the green dotted line.

tained more than $10^8$ copies of OBP-401, whereas the number of viral genomes was at the baseline level in nonmetastatic GFP-negative lymph nodes (Fig. 2C). The trafficking and replication ability of the virus was also confirmed in an orthotopic head and neck cancer xenograft model (see Figure, Supplemental Digital Content 3, online only, available at: http://links.lww.com/SLA/A40, which demonstrates OBP-401 virus spread delivered into primary tumors).

## Establishment of Highly Sensitive Quantitative Detection Assay for Lymph Node Metastasis

To achieve the highest sensitivity for detecting metastatic human tumor cells in mouse lymph nodes, we applied a novel quantitative real-time PCR assay that uses primer sets to amplify the consensus human *Alu* sequence.[18–20] *Alu* repeat sequences are specific to all human cells and are completely absent in mouse tissues.[21] To test the sensitivity and range of the assay, mouse splenocytes obtained from athymic *nu*/*nu* mice were spiked with variable numbers of HT29 human colorectal cancer cells in vitro (see Figure, Supplemental Digital Content 4A, online only, available at: http://links.lww.com/SLA/A41, which illustrates schematic procedures of detection and quantification of human cancer cells in mouse splenocytes). The total genomic DNA was extracted from the mixtures and subjected to quantitative *Alu*PCR. We also used the human *GAPDH* gene as an internal control to normalize the *Alu* signal in each sample. By plotting the *Alu*/*GAPDH* ratio as a function of the number of spiked tumor cells, a standard curve could be generated with a linear range between $10^3$ and $10^8$ cells, and regression analysis of the *Alu*/*GAPDH* ratio *versus* the number of expected tumor cells yielded a correlation coefficient of $R^2 = 0.9942$ ($P < 0.01$) (Fig. 3A). These results suggest that the *Alu*/*GAPDH* ratio reflects the actual human tumor cells among mouse splenocytes.

To verify the accuracy and sensitivity of the assay in vivo, we extracted DNA from total lymph nodes at different time points after the orthotopic implantation of HT29 cells and subjected the DNA to the *Alu*PCR analysis (see Figure, Supplemental Digital Content 4B,

online only, available at: http://links.lww.com/SLA/A41, which illustrates schematic procedures of detection and quantification of human cancer cells in mouse tissues). Then, we compared the *Alu/GAPDH* ratios and the metastatic rates determined with GFP expression by injection of OBP-401 into the primary rectal tumors 5 days before lymph node isolation. The *Alu/GAPDH* ratio showed a linear increase in a time-dependent manner, as the GFP-positive metastatic lymph node rate gradually increased (Fig. 3B). By calculating the estimated number of tumor cells according to the standard curve, we also demonstrated the time-dependent logarithm increase in metastatic human tumor cells in mouse lymph nodes (see Figure, Supplemental Digital Content 5, online only, available at: http://links.lww.com/SLA/A42, which demonstrates quantitative analysis of time-dependent development of spontaneous lymph node metastasis). Moreover, when HT29 tumor-bearing mice received a single intratumoral injection of OBP-401, the number of *Alu* copies was clearly correlated with the number of *E1A* copies in isolated mouse lymph nodes ($R^2 = 0.982$, $P < 0.01$), because telomerase-specific oncolytic adenovirus replicates only in metastatic tumor cells (Fig. 3C).

## Histologic Evaluation of the In Vivo Antitumor Effect of Virus on Lymph Node Metastasis

We next examined the in vivo antitumor effect of OBP-301 injected into the primary tumors on the regional lymph node metastasis. Mice bearing orthotopic HT29 rectal tumors with a diameter of 7 to 10 mm received 3 courses of intratumoral injections of $10^8$ plaque forming units (PFU) of OBP-301 or dl312, or PBS (mock treatment), every 2 days beginning on day 14 after the tumor inoculation. Histopathological examination of the excised total lymph nodes on day 35 showed that OBP-301 treatment considerably reduced the metastatic rates compared with that of mock-treated group, although replication-deficient dl312 had no apparent effects (Fig. 4A) (see Table, Supplemental Digital Content 6, online only, available at: http://links.lww.com/SLA/A43, which demonstrates histologic evaluation of antitumor effect of OBP-301 on lymph node metastasis). We also confirmed that OBP-301 significantly lowered the lymph node metastatic rates by averaging the histologically determined metastasis rates in individual mice ($P < 0.05$) (Fig. 4B). Representative histopathological images of lymph nodes with or without metastatic foci composed of HT29 tumor cells are shown in Figure 4C.

## Quantitative Evaluation of the In Vivo Antitumor Effect of Virus on Lymph Node Metastasis

By using a highly sensitive quantitative *Alu*PCR assay, we next investigated the antitumor effect of OBP-301 injected into the primary tumors on lymph node metastasis, which might be histopathologically undetectable. Mice received 3 courses of injections of $10^8$ PFU of OBP-301, $10^8$ PFU of dl312, or PBS (mock treatment) into orthotopic HT29 rectal tumors every 2 days beginning on day 14 after tumor inoculation. The *Alu* real-time PCR assay of isolated lymph nodes on day 35 demonstrated that mice treated with OBP-301 exhibited significantly fewer metastatic tumor cells as compared with dl312- or mock-treated mice (Fig. 5A). A more profound antitumor effect was achieved by increasing the number of injection cycles from 3 to 5 (see Figure, Supplemental Digital Content 7, online only, available at: http://links.lww.com/SLA/A44, which demonstrates quantitative analysis of antitumor effect of OBP-301 on lymph node metastasis). As expected, regional lymph nodes obtained from OBP-301-treated mice contained more *E1A* copies than the lymph nodes of mock-treated mice (Fig. 5B), suggesting that intratumorally delivered OBP-301 could spread and selectively replicate in metastatic lymph nodes.

We also used OBP-401 and the IVIS imaging system to assess the in vivo antitumor effect of OBP-301 on lymph node metastasis. After 14 days of orthotopic implantation of HT29 cells, OBP-301 ($1 \times 10^8$ PFU/body) was administered intratumorally for 5 cycles. We then used the IVIS imaging system to explore the abdominal cavity at laparotomy on day 35 following a single injection of OBP-401 ($1 \times 10^8$ PFU/body) into HT29 rectal tumors on day 30 (see Figure, Supplemental Digital Content 8, online only, available at: http://links.lww.com/SLA/A45, which illustrates schematic procedures of quantitative imaging of lymph node metastasis by the IVIS system). The number of GFP-positive lymph nodes and the GFP signal levels of individual lymph nodes were much higher in mock-treated control mice than in OBP-301-treated mice (Fig. 6A). Indeed, the sum of GFP fluorescence intensity in the abdominal cavity was significantly lower in mice treated with OBP-301 as compared with the mock-treated group, confirming the in vivo biologic purging effect of OBP-301 (Fig. 6B).

## Preoperative Purging Efficacy of Oncolytic Virotherapy against Lymph Node Metastasis

To compare the local control rates of virotherapy and radiotherapy for lymph node metastasis, mice bearing orthotopic HT29 tumors were treated with an intratumoral injection of $10^8$ PFU of

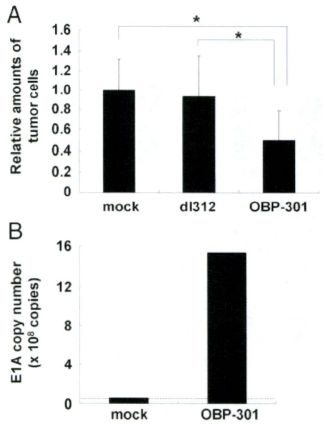


**FIGURE 5.** Quantitative PCR analysis of the antitumor effect of OBP-301 on lymph node metastasis in an orthotopic colorectal cancer xenograft model. A, Mice with established orthotopic HT29 tumors were treated with intratumoral injection of $1 \times 10^8$ PFU of OBP-301 or dl312 every 2 days for 3 cycles starting on day 14 after tumor inoculation. Lymph nodes were harvested on day 35, and then DNA was extracted and subjected to the quantitative *Alu*PCR analysis. The number of metastatic tumor cells is defined as the *Alu/GAPDH* ratio relative to that of the mock-treated sample (mock = 1). Data are shown as the mean ± SEM of 3 separate experiments. Statistical significance was defined as $P < 0.05$ (single asterisk). B, Genomic DNA extracted from lymph nodes of mice that received OBP-301 or PBS was also analyzed with real-time PCR targeting *E1A* to quantify the viral replication. A dotted line represents the baseline level.

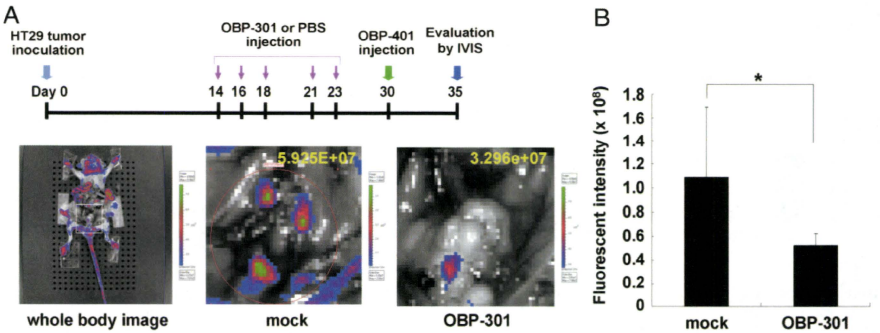


**FIGURE 6.** Quantitative imaging of lymph node metastasis to evaluate the antitumor effect of OBP-301 in an orthotopic colorectal cancer xenograft model. A, Quantitative imaging of lymph node metastasis by the IVIS system. Mice bearing HT29 xenograft tumors were treated with 5 cycles of intratumoral delivery of $1 \times 10^8$ PFU of OBP-301, followed by injection of OBP-401 ($10^8$ PFU) into HT29 tumors. Five days later, mice were killed and GFP expression was quantitated at laparotomy by IVIS camera (see Figure, Supplemental Digital Content 8, available at: http://links.lww.com/SLA/A45, which illustrates schematic procedures of quantitative imaging of lymph node metastasis by the IVIS system). B, GFP expression was measured as the mean photon flux in mock- and OBP-301-treated groups. A single asterisk indicates a statistically significant difference as compared with the mock-treated group.

OBP-301 or lower hemi-body ionizing radiation at a dosage of 3.3 Gy every 2 days for 3 cycles starting 14 days after tumor inoculation (see Figure, Supplemental Digital Content 9, online only, available at: http://links.lww.com/SLA/A46, which illustrates schematic procedures of quantitative PCR evaluation). The *Alu*PCR analysis of isolated lymph nodes at day 35 demonstrated that both intratumoral administration of OBP-301 and radiation equally resulted in a significant suppression of lymph node metastasis compared with mock-treated mice (Fig. 7A). However, regarding the adverse effects, the lower hemi-body irradiation targeting the regional para-aortic lymph nodes induced a significant body weight loss in mice approximately 10 to 14 days after treatment, whereas there were no apparent adverse effects in mice injected with OBP-301 during the observation period (data not shown). These results suggest that oncolytic virotherapy is less toxic than regional radiotherapy, although the antitumor effects of both approaches may be equivalent.

Finally, we examined whether preoperative intratumoral administration of OBP-301 had an antitumor effect against lymph node metastasis following the primary tumor resection. Mice bearing orthotopic HT29 tumors received intratumoral injections of $10^8$ PFU of OBP-301 every 2 days for 3 cycles starting 10 days after tumor inoculation. After primary rectal tumors were surgically removed on day 15, regional para-aortic lymph nodes were isolated on day 35, and then subjected to the *Alu*PCR analysis (see Figure, Supplemental Digital Content 9, online only, available at: http://links.lww.com/SLA/A46, which illustrates schematic procedures of quantitative PCR evaluation). The surgical resection of primary tumors caused considerable enhancement of lymph node metastasis; the preoperative treatment with OBP-301, however, not only inhibited the increase of lymphatic metastasis, but also significantly reduced lymph node metastasis compared with mock-treated mice (Fig. 7B). Images of representative mice before and after primary tumor resection are shown in Figure 7C. As implanted HT29 cells formed submucosal tumors with a solid architecture, tumors could be successfully excised with an incision in the anorectal wall (Fig. 7D).

## DISCUSSION

Lymph node metastases represent an aggressive tumor behavior and are associated with a high rate of regional recurrence, which portends a poor outcome and may produce marked morbidity.[1–3] Therefore, it would be clinically beneficial to eliminate or prevent lymph node metastasis to yield a better prognosis for cancer patients. Despite advances in surgical procedures of extended lymphadenectomy,[4,5] a more effective and less invasive management of lymphatic metastasis is needed. Here we describe a new, simple, and robust strategy that uses the telomerase-specific, replication-selective, oncolytic adenovirus OBP-301 to suppress tumor cell dissemination to regional lymph nodes in an orthotopic human colorectal cancer xenograft model.

The therapeutic potential of viral agents against primary tumors as well as their systemic biodistribution targeting distant metastases has been intensively investigated.[8,9,22] Few studies, however, have examined the ability of the virus to traffic to the regional draining lymph nodes. Recently, Burton et al showed that replication-deficient adenovirus could be successfully transported to the regional lymph nodes and noninvasively detect metastasis by expressing the prostate-specific reporter gene in an orthotopic prostate xenograft.[17] We have also previously demonstrated that intratumoral injection of the telomerase-specific, replication-selective, GFP-expressing adenovirus OBP-401 could efficiently visualize metastatic lymph nodes with GFP fluorescence signals in human cancer xenograft models.[15,23] Although these previous studies suggest the possible application of the adenovirus vectors as a lymphotropic agent for the treatment of lymph node metastasis, this effect has not been tested prior to the present study.

In vitro purging experiments demonstrated that OBP-301 infection could selectively eliminate human tumor cells in the presence of human or mouse lymphocytes (Fig. 1). We used OBP-401 to visualize viable human tumor cells after purging with OBP-301, as we have previously shown the high sensitivity and specificity

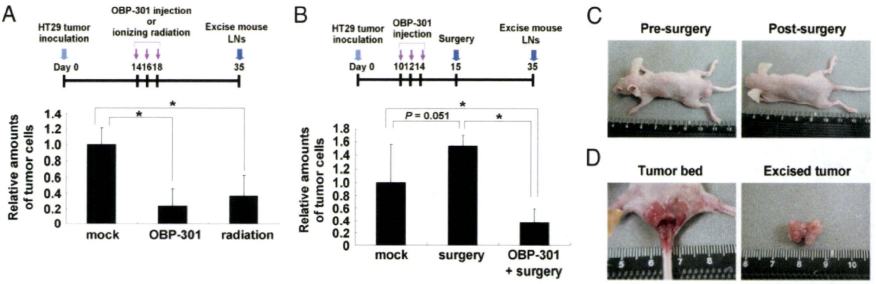


**FIGURE 7.** Comparative analysis of OBP-301 virotherapy with radiotherapy and surgery. A, In vivo purging effects of regional therapy with OBP-301 or ionizing irradiation on lymph node metastasis. Mice bearing HT29 xenograft tumors received 3 cycles of either intratumoral administration of OBP-301 ($10^8$ PFU) or lower hemibody irradiation starting at day 14 after tumor inoculation. Radiation was given every 2 days in 3.3-Gy fractions for a total dose of 10 Gy/mouse (see Figure, Supplemental Digital Content 9, available at: http://links.lww.com/SLA/A46, which illustrates schematic procedures of quantitative PCR evaluation). The number of metastatic tumor cells in mouse lymph nodes isolated on day 35 is defined as the *Alu*/*GAPDH* ratio relative to that of the mock-treated sample (mock = 1). Data are shown as the mean ± SEM of 3 separate experiments. Statistical significance was defined as $P < 0.05$ (single asterisk). (B) Preoperative purging effect of OBP-301 on lymph node metastasis. HT29 tumor-bearing mice were intratumorally injected with either $10^8$ PFU of OBP-301 or PBS on days 10, 12, and 14 after tumor inoculation. Primary HT29 tumors were surgically removed on day 15. The relative amount of HT29 tumor cells in mouse lymph nodes isolated on day 35 was assessed by the *Alu*PCR assay (see Figure, Supplemental Digital Content 9, available at: http://links.lww.com/SLA/A46, which illustrates schematic procedures of quantitative PCR evaluation). Note that the preoperative intratumoral administration of OBP-301 significantly (single asterisk: $P < 0.05$) reduced the number of metastatic tumor cells as compared with untreated or surgically treated mice. C, External images of orthotopic HT29 tumor-bearing *nu/nu* mice before and after surgical removal of the primary tumor. D, Macroscopic appearance of the tumor bed after surgical resection of the primary tumor, and the excised HT29 tumor.

of this molecular imaging method.[15,23] It has been reported that the fiber-modified adenovirus serotype 5 (Ad5) and the adenovirus vector based on another serotype such as 35 efficiently transduce exogenous genes into hematopoietic cells, including stem cells; the unmodified Ad5, however, could rarely infect these cells because of the lack of the coxsackievirus and adenovirus receptor expression.[24] Indeed, Ad5-based OBP-301 had no apparent effects on the viability of lymphocytes in vitro. These results suggest that normal lymphocytes in the regional lymph nodes could be strictly protected from OBP-301-induced oncolysis, because lymphocytes are not permissive for OBP-301 infection and viral replication is also unlikely to occur in normal cells due to their low telomerase activity.[25]

Previously, we used serial tissue sections of mouse lymph nodes stained with hematoxylin and eosin to detect microscopic metastasis; this time-consuming technique, however, is not quantitative.[15,23] To quantify the few metastatic human tumor cells in a background of large numbers of mouse host cells, a simple real-time *Alu*PCR assay was developed in the current study. This human-specific amplification method enabled us to detect human tumor cells in a linear range of $10^3$ to $10^8$ cells/sample and monitor the time-dependent exponential growth of spontaneous lymph node metastasis from orthotopic colorectal tumor xenografts (Fig. 3). In accordance with the histologically confirmed results, the *Alu*PCR assay indicated that intratumoral injection of OBP-301 into the primary tumors significantly inhibited lymph node metastasis with high levels of viral replication (Figs. 4, 5). We also used the previously established OBP-401-mediated in vivo imaging in combination with a 3-dimensional optical detection system (IVIS 200) to demonstrate a significant suppressive effect of OBP-301 against lymph node metastasis (Fig. 6). The fact that 2 independent and highly sensitive approaches showed comparable results suggests a potent in vivo purging effect of oncolytic virotherapy on regional lymph nodes.

Currently, surgery and radiation are the most effective and clinically reliable local management strategies for human malignancies including lymphatic metastases. Indeed, ionizing radiation targeting the lower half of the mouse body including primary tumors and the para-aortic lymphatic area significantly inhibited lymph node metastasis (Fig. 7A), although the systemic toxicity such as the body weight loss was remarkable in irradiated mice compared with mice treated with OBP-301 (data not shown). In fact, a total body irradiation at a dose of 10 Gy has been reported to be lethal in mice because of acute radiation syndromes involving the hematopoietic system and gastrointestinal tract.[26] In this regard, our data clearly indicate that regional oncolytic virotherapy might be more simple and safe than radiotherapy as a treatment for metastatic lymph nodes. We also assessed the effect of surgical resection of primary rectal tumors on lymph node metastasis. Unexpectedly, metastatic tumor cells in the lymph nodes considerably increased after surgical removal of primary tumors, presumably due to the excessive load to the host. Another possible explanation of this phenomenon includes a decrease in angiogenic inhibitors such as angiostatin and endostatin secreted from the primary tumor mass.[27] In contrast, intratumoral injection of OBP-301 prior to surgical resection significantly inhibited lymph node metastasis (Fig. 7B), suggesting that, although the surgical procedure itself has the potential to promote regional metastasis, the preoperative treatment with OBP-301 may prevent this undesirable event.

## CONCLUSION

The highly sensitive PCR assay targeting the human *Alu* sequence has shown that the oncolytic adenovirus delivered to the

primary tumor site could spread into the regional draining lymphatics, selectively replicate in neoplastic foci, and then reduce the number of tumor cells in metastatic lymph nodes in an orthotopic human colorectal cancer xenograft model. This virus-mediated molecular surgery for lymph node metastasis mimics the clinical scenario of lymphadenectomy; the technique, however, seems to be safer and less invasive. Moreover, we demonstrated that preoperative delivery of OBP-301 into primary tumors prevented the exacerbation of lymph node metastasis by surgical procedures. OBP-301 may offer advantages over other oncolytic viruses targeting lymphatic metastasis, as its safety profile as well as biodistribution pattern after intratumoral delivery have already been confirmed in a phase I clinical trial for various types of solid tumors.[14] The current study provides evidence for the in vivo purging effect of OBP-301 in regional lymph nodes that is sufficiently reliable to support this approach. Thus, phase II studies of telomerase-specific virotherapy targeting lymph node metastasis in human cancer patients are warranted.

## ACKNOWLEDGMENTS

*The authors thank Daiju Ichimaru (Oncolys BioPharma, Inc.) for the helpful discussion. The authors also thank Tomoko Sueishi and MitsukoYokota for the excellent technical support.*

## REFERENCES

1. Maehara Y, Oshiro T, Endo K, et al. Clinical significance of occult micrometastasis lymph nodes from patients with early gastric cancer who died of recurrence. *Surgery*. 1996;119:397–402.
2. Rivadeneira DE, Simmons RM, Christos PJ, et al. Predictive factors associated with axillary lymph node metastases in T1a and T1b breast carcinomas: analysis in more than 900 patients. *J Am Coll Surg*. 2000;191:1–6.
3. Chang GJ, Rodriguez-Bigas MA, Skibber JM, et al. Lymph node evaluation and survival after curative resection of colon cancer: systematic review. *J Natl Cancer Inst*. 2007;99:433–441.
4. Volpe CM, Koo J, Miloro SM, et al. The effect of extended lymphadenectomy on survival in patients with gastric adenocarcinoma. *J Am Coll Surg*. 1995;181:56–64.
5. Harrison LE, Karpeh MS, Brennan MF. Extended lymphadenectomy is associated with a survival benefit for node-negative gastric cancer. *J Gastrointest Surg*. 1998;2:126–131.
6. Sasako M, Sano T, Yamamoto S, et al. D2 lymphadenectomy alone or with para-aortic nodal dissection for gastric cancer. *N Engl J Med*. 2008;359:453–462.
7. Gotoda T, Sasako M, Ono H, et al. Evaluation of the necessity for gastrectomy with lymph node dissection for patients with submucosal invasive gastric cancer. *Br J Surg*. 2001;88:444–449.
8. Liu TC, Galanis E, Kirn D. Clinical trial results with oncolytic virotherapy: a century of promise, a decade of progress. *Nat Clin Pract Oncol*. 2007;4:101–117.
9. Kirn DH, Thorne SH. Targeted and armed oncolytic poxviruses: a novel multi-mechanistic therapeutic class for cancer. *Nat Rev Cancer*. 2009;9:64–71.
10. Fujiwara T. Telomerase-specific virotherapy for human squamous cell carcinoma. *Expert Opin Biol Ther*. 2009;9:321–329.
11. Kawashima T, Kagawa S, Kobayashi N, et al. Telomerase-specific replication-selective virotherapy for human cancer. *Clin Cancer Res*. 2004;10:285–292.
12. Umeoka T, Kawashima T, Kagawa S, et al. Visualization of intrathoracically disseminated solid tumors in mice with optical imaging by telomerase-specific amplification of a transferred green fluorescent protein gene. *Cancer Res*. 2004;64:6259–6265.
13. Taki M, Kagawa S, Nishizaki M, et al. Enhanced oncolysis by a tropism-modified telomerase-specific replication-selective adenoviral agent OBP-405 (Telomelysin-RGD). *Oncogene*. 2005;24:3130–3140.
14. Fujiwara T, Tanaka N, Numunaitis JJ, et al. Phase I trial of intratumoral administration of OBP-301, a novel telomerase-specific oncolytic virus, in patients with advanced solid cancer: evaluation of biodistribution and immune response. *J Clin Oncol*. 2008;26:3572.
15. Kishimoto H, Kojima T, Watanabe Y, et al. In vivo imaging of lymph node metastasis with telomerase-specific replication-selective adenovirus. *Nat Med*. 2006;12:1213–1219.
16. Johnson M, Huyn S, Burton J, et al. Differential biodistribution of adenoviral vector in vivo as monitored by bioluminescence imaging and quantitative polymerase chain reaction. *Hum Gene Ther*. 2006;17:1262–1269.
17. Burton JB, Johnson M, Sato M, et al. Adenovirus-mediated gene expression imaging to directly detect sentinel lymph node metastasis of prostate cancer. *Nat Med*. 2008;14:882–888.
18. Schneider T, Osl F, Friess T, et al. Quantification of human Alu sequences by real-time PCR—an improved method to measure therapeutic efficacy of anti-metastatic drugs in human xenotransplants. *Clin Exp Metastasis*. 2002; 19:571–582.
19. Zijlstra A, Mellor R, Panzarella G, et al. A quantitative analysis of rate-limiting steps in the metastatic cascade using human-specific real-time polymerase chain reaction. *Cancer Res*. 2002;62:7083–7092.
20. Umetani N, Giuliano AE, Hiramatsu SH, et al. Prediction of breast tumor progression by integrity of free circulating DNA in serum. *J Clin Oncol*. 2006;24:4270–4276.
21. Kariya Y, Kato K, Hayashizaki Y, et al. Revision of consensus sequence of human Alu repeats—a review. *Gene*. 1987;53:1–10.
22. Liu TC, Kirn D. Systemic efficacy with oncolytic virus therapeutics: clinical proof-of-concept and future directions. *Cancer Res*. 2007;67:429–432.
23. Kurihara Y, Watanabe Y, Onimatsu H, et al. Telomerase-specific virotheranostics for human head and neck cancer. *Clin Cancer Res*. 2009;15:2335–2343.
24. Kawabata K, Sakurai F, Koizumi N, et al. Adenovirus vector-mediated gene transfer into stem cells. *Mol Pharm*. 2006;3:95–103.
25. Hiyama K, Hirai Y, Kyoizumi S, et al. Activation of telomerase in human lymphocytes and hematopoietic progenitor cells. *J Immunol*. 1995;155:3711–3715.
26. Burdelya LG, Krivokrysenko VI, Tallant TC, et al. An agonist of toll-like receptor 5 has radioprotective activity in mouse and primate models. *Science*. 2008;320:226–230.
27. Folkman J. Role of angiogenesis in tumor growth and metastasis. *Semin Oncol*. 2002;29:15–18.

 

*Research Article*

Molecular Cancer Therapeutics

# Preclinical Evaluation of Differentially Targeting Dual Virotherapy for Human Solid Cancer

Ryo Sakai[1], Shunsuke Kagawa[1,2], Yasumoto Yamasaki[1], Toru Kojima[1], Futoshi Uno[1,2], Yuuri Hashimoto[1,3], Yuichi Watanabe[1,3], Yasuo Urata[3], Noriaki Tanaka[1], and Toshiyoshi Fujiwara[1,2]

## Abstract

Multimodal approaches combining drugs that differentially function is the most popular regimen for treating human cancer. Understanding the molecular mechanisms underlying the synergistic, potentiative, and antagonistic effects of drug combinations could facilitate the discovery of novel efficacious combinations. We previously showed that telomerase-specific replication-competent adenovirus (Telomelysin, OBP-301), in which the human telomerase reverse transcriptase promoter controls the adenoviral E1 gene expression, induces a selective antitumor effect in human cancer cells. Here, using E1-deleted replication-deficient adenovirus expressing the p53 tumor suppressor gene (Advexin, Ad-p53) and OBP-301, we investigate how these adenoviruses that kill tumor cells with different mechanisms could work in combination on human cancer. We found that E1-deficient Ad-p53 could kill cancer cells more efficiently in the presence of OBP-301 than Ad-p53 alone or OBP-301 alone, because Ad-p53 could become replication-competent by being supplied adenoviral E1 from coinfected OBP-301 in trans. Ad-p53 plus OBP-301 induced high levels of p53 protein expression without p21 induction, resulting in apoptotic cell death documented by active caspase-3 expression with a cytometric bead array and an increased subdiploid apoptotic fraction of the cell cycle. For *in vivo* evaluation, nude mice xenografted with human lung tumors received intratumoral injection of OBP-301 and/or Ad-p53. Analysis of the growth of implanted tumors showed an enhanced antitumor effect in combination therapy. Our data show that Ad-p53 in combination with OBP-301 induces not only oncolytic but also apoptotic cancer cell death and enhances antitumor activity *in vitro* and *in vivo*, providing potential merits as a multimodal treatment for human cancer. *Mol Cancer Ther; 9(6); 1884–93. ©2010 AACR.*

## Introduction

Combining antineoplastic agents with different mechanisms of action has resulted in many effective regimens in cancer therapy. For example, biochemical modulation of 5-fluorouracil, one of the most active single agents presently available, with the reduced folate leucovorin has significantly improved overall response rates in the 25% to 30% range (1). To successfully achieve synergistic effects, we need to elucidate the biochemical and/or molecular mechanisms underlying the drug interaction. Recent advances in understanding the molecular mechanisms of carcinogenesis allow us to develop a number of molecularly targeted therapies. Most agents have been developed to target specific molecules which are essential for the acquisition of malignant phenotypes such as proliferation, invasion, and metastasis.

Gene- and vector-based therapies, which have long been viewed as unsuccessful, have been greatly rejuvenated by its combination with other modalities including chemotherapy and radiotherapy (2, 3). It also remains possible to increase the therapeutic benefit by combining virotherapies having different targets. Ad-p53 (Advexin, Ad5CMV-p53) consists of an E1-deleted replication-deficient type 5 adenoviral vector expressing the human wild-type p53 tumor suppressor gene under the control of a cytomegalovirus promoter. p53 is the most commonly mutated gene in human cancer (4, 5), and p53 gene therapy using Ad-p53 is currently in clinical trials as a cancer therapy (6–9); however, a number of limitations have led to the suboptimal efficacy of existing gene therapies. One reason is that replication-deficient adenoviruses infect only a small portion of the tumor and are not able to spread over the tumor entirely. To improve viral spread in tumor conferring specificity of infection, replication-competent adenoviruses have been investigated (10–12).

**Authors' Affiliations:** [1]Department of Gastroenterological Surgery, Okayama University Graduate School of Medicine, Dentistry, and Pharmaceutical Sciences, [2]Center for Gene and Cell Therapy, Okayama University Hospital, Okayama, Japan; and [3]Oncolys BioPharma, Inc., Tokyo, Japan

**Corresponding Author:** Toshiyoshi Fujiwara, Department of Gastroenterological Surgery, Okayama University Graduate School of Medicine, Dentistry, and Pharmaceutical Sciences, 2-5-1 Shikata-cho, Kita-ku, Okayama 700-8558, Japan. Phone: 81-86-235-7257; Fax: 81-86-221-8775. E-mail: toshi_f@md.okayama-u.ac.jp

**doi:** 10.1158/1535-7163.MCT-10-0205

We previously developed a telomerase-specific, replication-competent adenovirus (Telomelysin, OBP-301), in which the human telomerase reverse transcriptase (hTERT) promoter element drives the adenoviral E1 gene, and induced a selective antitumor effect in human cancer cells (13–17). Telomerase is a ribonucleoprotein complex responsible for the complete replication of chromosomal ends (18). Many studies have shown the expression of telomerase activity in more than 85% of human cancers (19), but only in few normal somatic cells (20). Telomerase activation is considered a critical step in carcinogenesis and its activity is closely correlated with hTERT expression (21). Although virotherapy using OBP-301 as a monotherapy is currently being evaluated in clinical trials (22), multimodal strategies to enhance antitumor efficacy *in vivo* might be essential for a successful clinical outcome.

As a replication-deficient adenovirus could replicate in cancer cells and enhance the anticancer effect when cotransfected with a replication-competent adenovirus that could produce E1 proteins, we reasoned that combined treatment with Ad-p53 and OBP-301 might offer a way to more efficiently kill human tumor cells. In the present study, we investigated the synergistic effects of Ad-p53 combined with OBP-301 both *in vitro* and *in vivo*.

## Materials and Methods

### Cell lines and cell cultures

The human non–small cell lung cancer cell line H1299, which has a homozygously deleted p53, and the human colorectal carcinoma cell line SW620, which contains mutated p53, were propagated in monolayer culture in RPMI 1640 supplemented with 10% FCS, 100 units/mL of penicillin, and 100 μg/mL of streptomycin.

### Recombinant adenoviruses

The recombinant replication-selective, tumor-specific adenovirus vector OBP-301 (Telomelysin), in which the hTERT promoter element drives the expression of E1A and E1B genes linked with an IRES, was constructed and characterized previously (16). Replication-deficient adenoviral vectors containing human wild-type p53 cDNA (Ad-p53) and β-galactosidase cDNA (Ad-lacZ) were also used (23). These viruses were purified by $CsCl_2$ step gradient ultracentrifugation followed by $CsCl_2$ linear

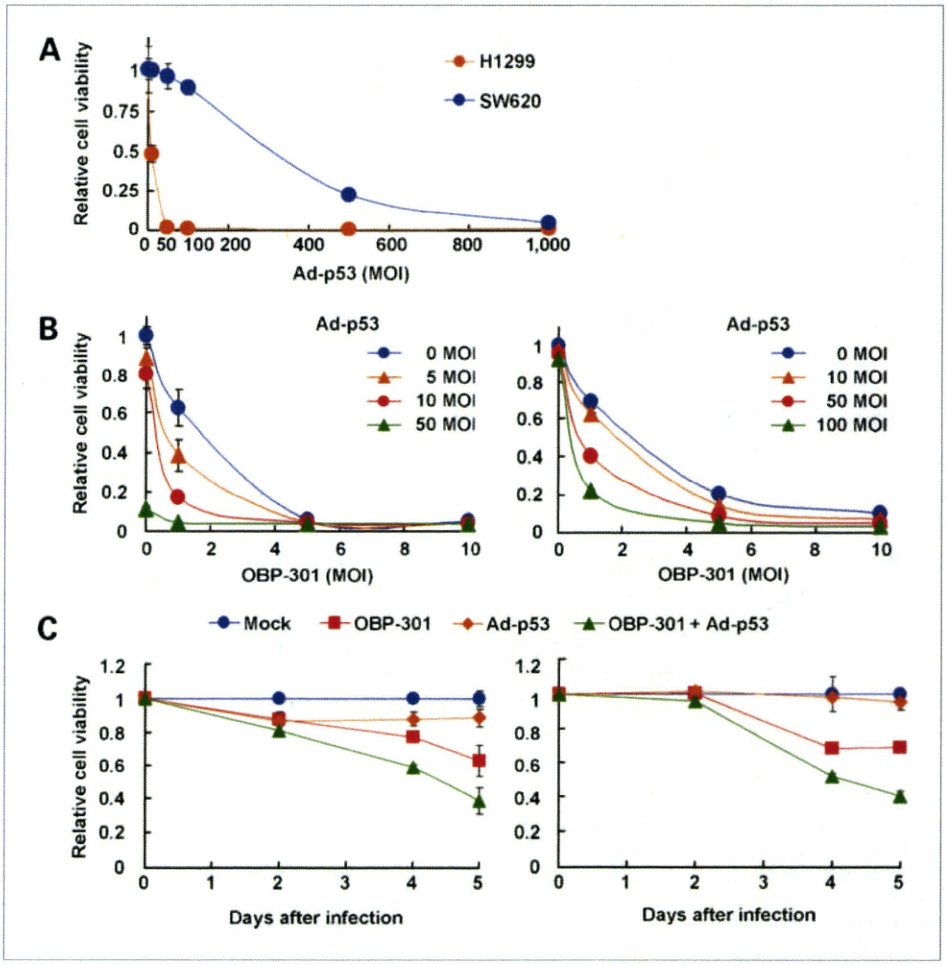


Figure 1. A, effect of Ad-p53 on human cancer cell lines. H1299 and SW620 cells were infected with 0, 10, 50, 100, 500, and 1,000 MOIs of Ad-p53. Cell viability was assessed by XTT assay 5 d after infection. B, dose-response analysis of cell viability in combination therapy. H1299 (left) and SW620 (right) cells were treated with the indicated MOIs of Ad-p53, OBP-301, or a combination of both simultaneously. The cell-killing effect was evaluated by XTT assay 5 d after infection. C, time course analysis of cell viability in combination therapy. H1299 (left) and SW620 (right) cells were treated with 1 MOI of OBP-301, 5 MOI (for H1299) or 50 MOI (for SW620) of Ad-p53, or a combination of both at the same time. Cell viability was assessed by XTT assay 2, 4, and 5 d after infection. Bars, SD.

gradient ultracentrifugation, and their titers were determined by plaque assay in the 293 cells.

### Cell proliferation assay

Cells were seeded at 1,000 cells/well in 96-well plate and infected with OBP-301, Ad-p53, or OBP-301 and Ad-p53 simultaneously at the indicated multiplicities of infection (MOI) 18 to 20 hours later. Cell viability was assessed at the indicated times after adenoviral infection using sodium 3′-[1-(phenylaminocarbonyl)-3,4-tetrazolium]-bis(4-methoxy-6-nitro) benzene sulfonic acid hydrate (XTT) assay with the Cell Proliferation Kit II (Roche Molecular Biochemicals) according to the protocol provided by the manufacturer.

### Western blot analysis

The primary antibodies against p53 (Ab-2; Calbiochem), p21 (EA10; Oncogene Science), β-actin (AC-15; Sigma Chemical, Co.), and peroxidase-linked secondary antibody (Amersham) were used. Cells were washed twice in cold PBS and collected then lysed in lysis buffer [10 mmol/L Tris (pH 7.5), 150 mmol/L NaCl, 50 mmol/L NaF, 1 mmol/L EDTA, 10% glycerol, and 0.5% NP40] containing proteinase inhibitors (0.1 mmol/L phenylmethylsulfonyl fluoride and 0.5 mmol/L $Na_3VO_4$). After 20 minutes on ice, the lysates were spun at 14,000 rpm in a microcentrifuge at 4°C for 5 minutes. The supernatants were used as whole cell extracts. Protein concentration was determined using the Bio-Rad protein determination method (Bio-Rad). Equal amounts of proteins were boiled for 5 minutes and electrophoresed under reducing conditions in 4% to 12% (w/v) polyacrylamide gels. Proteins were electrophoretically transferred to Hybond polyvinylidene difluoride transfer membranes (Amersham Life Science) and incubated with the primary antibody followed by peroxidase-linked secondary antibody. An Amersham ECL chemiluminescent western system (Amersham) was used to detect secondary probes.

### Human apoptosis cytometric bead array for active caspase-3

Caspase-3 activation was quantitated using the Human Apoptosis Cytometric Bead Array kit (Becton Dickinson) according to the instructions of the manufacturer. Briefly, cell lysates were incubated with cytometric caspase-3 capture beads coated with antibody specific for caspase-3 and a secondary antibody specific for the cleaved site of active caspase-3 conjugated to phycoerythrin. Cytometric bead/caspase-3 conjugates were analyzed by flow cytometry using a FACSCalibur (Becton Dickinson). Flow cytometry measures the amount of active caspase-3 attached to beads. Becton Dickinson Cytometric Bead Array software was used to analyze beads and transform data from samples. Sample data

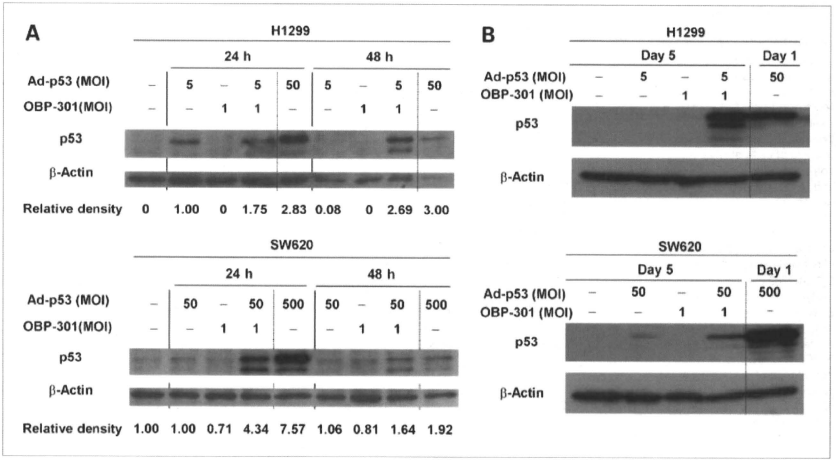


Figure 2. Expression of p53 in combination therapy of Ad-p53 and OBP-301. H1299 and SW620 cells were infected with the indicated viruses and harvested at the indicated time. Cell lysates were subjected to immunoblot analysis for p53 and β-actin. H1299 cells infected with 50 MOI of Ad-p53 and SW620 cells infected with 500 MOI of Ad-p53 were used as a positive control for apoptosis. A, cells were harvested in the early phase (24 and 48 h after infection). p53 expression level was quantified by densitometric scanning using NIH Image software and normalization by dividing the β-actin signal. The background was subtracted and corrected so that the control became 0, because H1299 cells were p53-null. B, cells were harvested in the late phase (5 d after infection).

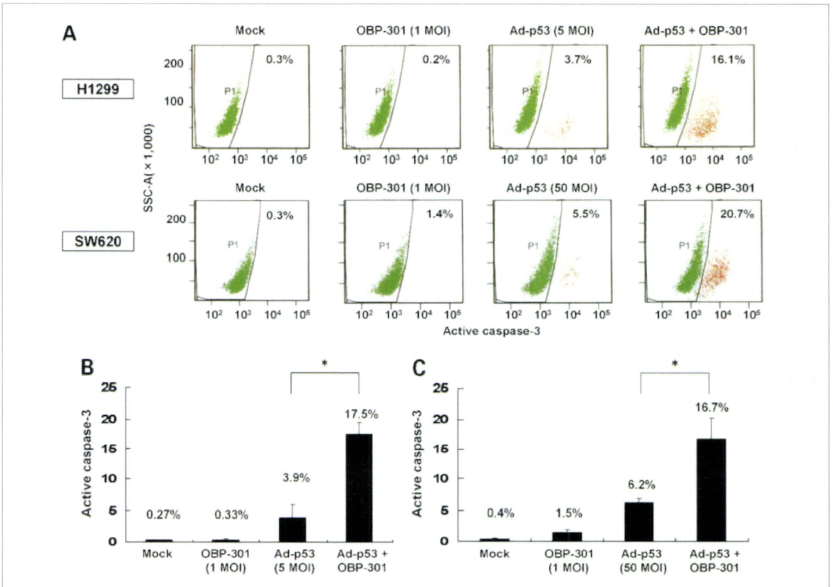


Figure 3. Induction of apoptosis in H1299 and SW620 cells following infection with Ad-p53 plus OBP-301. H1299 and SW620 cells were infected with the indicated MOIs of OBP-301, Ad-p53, or a combination of both simultaneously. Caspase-3 activation was quantitated using the cytometric bead array (CBA) assay 48 h after infection. A, representative flow cytometric images are shown. B and C, active caspase-3 expression was significantly increased after infection with Ad-p53 plus OBP-301 in H1299 (B) and SW620 (C) cells. Columns, mean of three experiments; bars, SE. *, $P < 0.01$, statistical significance (Student's $t$ test).

was normalized with specific protein standards to provide quantification of the proteins of interest.

### *In vitro* replication assay

H1299 cells were infected with OBP-301 (1 MOI), Ad-p53 (5 MOI), OBP-301 (1 MOI) + Ad-p53 (5 MOI), or OBP-301 (1 MOI) + Ad-lacZ (5 MOI) for 24 hours after seeding for 2 hours. Following the removal of virus inocula, the cells were further incubated at 37°C, trypsinized, and harvested at 2, 24, 48, and 72 hours after infection. DNA purification was done using QIAmp DNA mini kit (Qiagen, Inc.). The E1A and p53 DNA copy numbers were determined by quantitative real-time PCR using a LightCycler instrument and LightCycler-DNA Master SYBR Green I (Roche Diagnostics).

### Cell cycle analysis

Cells treated with various concentrations of OBP-301, Ad-p53, or a combination of both were harvested in 0.125% trypsin, washed twice in PBS with 2% FCS. After centrifugation, $1 \times 10^6$ cells were resuspended in 70% ethanol at 4°C overnight. Cells were washed twice in PBS. After centrifugation, the pellet was resuspended in 0.25 μg/mL of RNase A for 30 minutes at 37°C. The samples were then stained with 50 μg/mL of propidium iodide and incubated at 4°C for 30 minutes. Cell cycle analysis was determined by FACSCalibur flow cytometer using FlowJo software (TreeStar, Inc.).

### *In vivo* human tumor model

H1299 cells ($7.5 \times 10^6$ cells/mouse) were injected s.c. into the flank of 5-week-old female BALB/c *nu/nu* mice and permitted to grow to 4 to 10 mm in diameter. At that time, the mice were randomly assigned into six groups, and a 50 μL solution containing Ad-p53 [$1 \times 10^9$ plaque-forming units (pfu)], OBP-301($1 \times 10^7$ pfu), OBP-301 ($1 \times 10^7$ pfu) + Ad-p53 ($1 \times 10^8$ pfu), or Ad-lacZ ($1 \times 10^8$ pfu), Ad-p53 ($1 \times 10^8$ pfu) + Ad-lacZ ($1 \times 10^7$ pfu), or PBS was injected into the tumor for three cycles every 2 days. The perpendicular diameter of each tumor was measured every 3 or 4 days, and tumor volume was calculated using the following formula:

tumor volume ($mm^3$) = $a \times b^2 \times 0.5$, where $a$ is the longest diameter, $b$ is the shortest diameter and 0.5 is a constant to calculate the volume of an ellipsoid. The experimental protocol was approved by the Ethics Review Committee for Animal Experimentation of Okayama University School of Medicine.

### Statistical analysis

The statistical significance of the differences in the *in vitro* and *in vivo* antitumor effects of viruses was determined by using the (two-tailed) Student's *t* test.

## Results

### Enhanced antitumor effect of OBP-301 plus Ad-p53 in human cancer cell lines *in vitro*

To achieve optimum antitumor effect, Ad-p53 at the MOI of 50 and 500 was needed in H1299 and SW620 cells, respectively (Fig. 1A). We have previously confirmed that these cells expressed detectable hTERT mRNA (13, 14). To examine the potential interaction of Ad-p53 with OBP-301, we did a dose-response analysis of the cell-killing effect at various doses in H1299 and SW620 cells. Ad-p53 at 5 or 50 MOI could have little antitumor effect in H1299 and SW620 cells, respectively. Combination therapy with 1 MOI of OBP-301 plus Ad-p53 resulted in more cell killing than OBP-301 alone or Ad-p53 alone in both cells (Fig. 1B). In contrast, OBP-301 plus Ad-lacZ did not increase the antitumor effect (data not shown). We next examined a time course analysis of the cell-killing effect. The antitumor effect of Ad-p53 plus OBP-301 was augmented after 4 days of infection (Fig. 1C). To determine whether the timing of administration of the adenoviruses affected the combined cytotoxic effect, H1299 and SW620 cells were treated with Ad-p53 24 hours after infection or synchronously with OBP-301. The results showed no apparent differences in cytotoxic activity by the treatment schedules (data not shown).

### Increased expression of p53 by cotransduction with OBP-301 and Ad-p53

To explore the effect of the combination of Ad-p53 and OBP-301, the expression levels of p53 protein were compared by immunoblotting analyses at 24 and 48 hours after infection. By cotransduction with Ad-p53 and OBP-301, the expression of p53 was 33.6-fold higher in H1299 cells at 48 hours and 4.34-fold higher in SW620

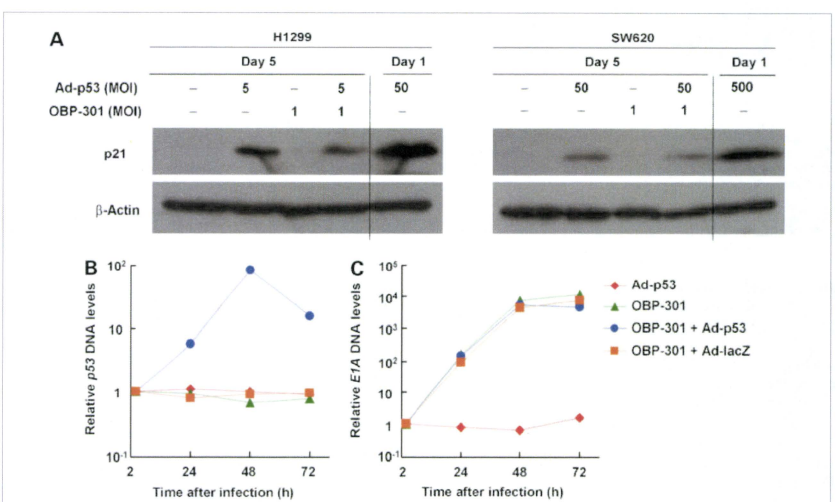


Figure 4. A, expression of p53 downstream mediator p21. H1299 and SW620 cells were infected with the indicated viruses and harvested at the indicated times. Cell lysates were subjected to immunoblot analyses for p21 and β-actin. H1299 cells infected with 50 MOI of Ad-p53 and SW620 cells infected with 500 MOI of Ad-p53 were used as a positive control for p21 induction. B and C, assessment of viral DNA replication in H1299 cells. H1299 cells were infected with OBP-301 (1 MOI), Ad-p53 (5 MOI), OBP-301 (1 MOI) + Ad-p53 (5 MOI), or OBP-301 (1 MOI) + Ad-lacZ (5 MOI) for 2 h. Following the removal of virus inocula, the cells were further incubated at 37°C, trypsinized, and harvested at 2, 24, 48, and 72 h after infection. Extracted DNA was subjected to real-time PCR assay for p53 DNA (B) and E1A DNA (C).

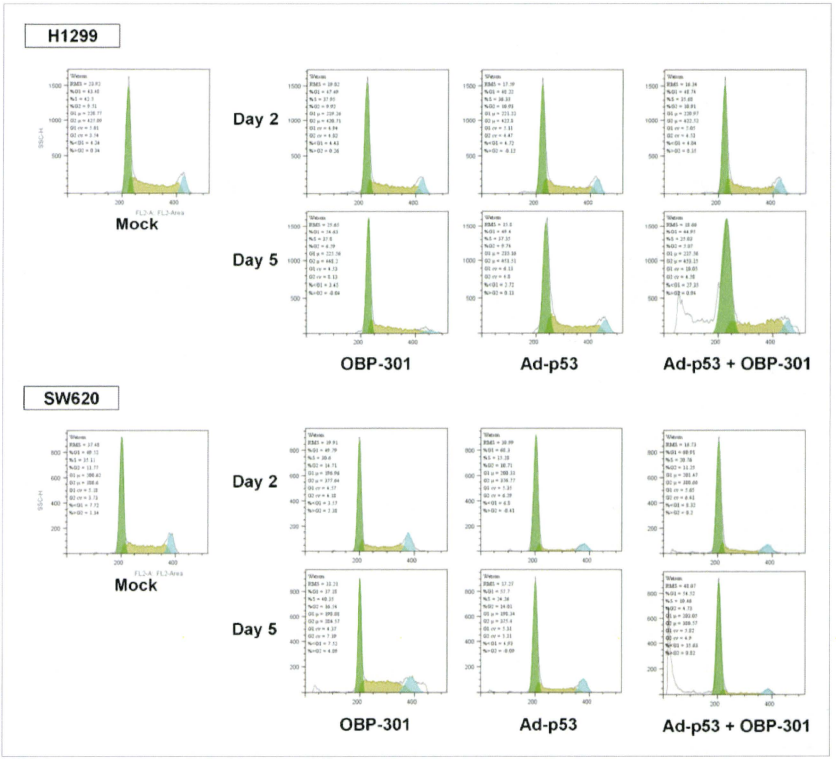


Figure 5. H1299 cells were infected with 1 MOI of OBP-301, 5 MOI of Ad-p53, or a combination of both and harvested on days 2 and 5. SW620 cells were infected with 1 MOI of OBP-301, 50 MOI of Ad-p53, or a combination of both and harvested on days 2 and 5. Cells were stained with propidium iodide. Then, cell cycle analysis was determined by the fluorescence-activated cell sorter (FACSCalibur) flow cytometer.

cells at 24 hours than by Ad-p53 alone (Fig. 2A). The augmented expression of p53 was maintained in cotransduced cells with both adenoviruses on day 5 (Fig. 2B). The prolonged upregulation of p53 suggests that Ad-p53 replicates in cancer cells by E1 protein supplied by cotransduced OBP-301, although the pattern of increased p53 expression was different between H1299 and SW620 cells. These cells expressed equivalent levels of coxsackievirus and adenovirus receptor (15); p53-null H1299 cells were, however, more sensitive to Ad-p53 compared with SW620 cells containing mutated p53, as shown in Fig. 1A, suggesting that Ad-p53 induced rapid apoptosis within 48 hours in infected H1299 cells and, therefore, p53 expression declined at 48 hours after infection. In contrast, as Ad-p53 could replicate and infect more H1299 cells in the presence of OBP-301, the level of p53 expression increased after coinfection of Ad-p53 and OBP-301.

### Combined treatment of OBP-301 plus Ad-p53 more efficiently induced apoptosis

Overexpression of p53 is known to induce apoptosis in most cancer cells. We hypothesized that the enhanced antitumor effect of Ad-p53 plus OBP-301 would result in elevated apoptotic cell death. Two days after infection, combined treatment of Ad-p53 plus OBP-301 induced significantly elevated levels of active caspase-3, whereas a low dose of Ad-p53 alone did not (Fig. 3). Moreover, interestingly, the expression level of p21, which is a

downstream target of p53 in combination therapy with OBP-301 and Ad-p53, was lower than in low doses of Ad-p53 alone (Fig. 4A).

### p53 DNA copy number is significantly amplified in combination therapy with OBP-301 and Ad-p53, whereas p53 does not impair the replication of OBP-301

Then we examined the p53 DNA levels in H1299 cells. The amplification of p53 DNA in the cells treated with Ad-p53 plus OBP-301 by one to two orders of magnitude was observed (Fig. 4B). These results suggest that Ad-p53 actually replicates by using the E1 protein supplied by OBP-301, which is consistent with increased expression of p53 protein (Fig. 2A). In this combination treatment, proapoptotic p53 expression might impair the replication of oncolytic virus because of premature early cell death provoked by p53. Therefore, we examined the effect of p53 on the replication of OBP-301 by quantitative real-time PCR analysis. H1299 cells were infected with OBP-301 and/or Ad-p53. Cells were harvested 2, 24, and 48 hours after infection, and extracted DNA were subjected to the assay. As shown in Fig. 4C, the presence of Ad-p53 did not impair the replication of OBP-301.

### Augmentation of apoptosis in human tumor cells after coinfection with Ad-p53 and OBP-301

We next did a cell cycle analysis in H1299 and SW620 cells on days 2 and 5 after infection. Neither group showed any differences between treatment 2 days after infection; however, a sub-$G_1$ population (an apoptotic cell population) was markedly increased in H1299 and SW620 cells infected with Ad-p53 plus OBP-301 after 5 days of infection, whereas OBP-301 or Ad-p53 alone did not increase apoptosis (Fig. 5; Table 1). These results were compatible with those of the time course analyses (Fig. 1C), suggesting that the augmented antitumor effect of combined treatment of Ad-p53 and OBP-301 was due to enhanced apoptotic cancer cell death.

### Antitumor effect of OBP-301 plus Ad-p53 in human tumor xenografts

Based on the *in vitro* combination effect of Ad-p53 and OBP-301, the *in vivo* therapeutic efficacy of H1299 tumors was further assessed. Mice bearing H1299-xenografted tumors measuring 4 to 10 mm in diameter received intratumoral injection of Ad-p53 at a dose of $1 \times 10^8$ pfu and OBP-301 at a dose of $1 \times 10^7$ pfu, singly or in combination every 2 days for three cycles starting at day 0. As shown in Fig. 6, Ad-p53 alone and Ad-p53 + Ad-lacZ had no apparent antitumor effect, but OBP-301 alone resulted in significant tumor suppression compared with controls ($P < 0.05$). OBP-301 plus Ad-lacZ did not improve the tumor suppression compared with OBP-301 alone ($P > 0.05$). Nevertheless, the combination of OBP-301 plus Ad-p53 produced a more profound and significant inhibition of tumor growth compared with OBP-301 alone or OBP-301 plus Ad-lacZ ($P < 0.05$).

**Table 1.** Cell cycle analysis following infection with OBP-301, Ad-p53, or Ad-p53 plus OBP-301 in H1299 and SW620 cells

| Cell lines | Days | Treatments | Cell cycle distribution (%) | | | |
|---|---|---|---|---|---|---|
| | | | Sub-$G_0$-$G_1$ | $G_0$-$G_1$ | S | $G_2$-M |
| H1299 | | Mock | 4.51 | 43.48 | 42.5 | 9.51 |
| | Day 2 | OBP-301 | 4.64 | 47.49 | 37.95 | 9.92 |
| | | Ad-p53 | 4.52 | 48.22 | 36.33 | 10.93 |
| | | Ad-p53 + OBP-301 | 4.67 | 48.74 | 35.68 | 10.91 |
| | Day 5 | OBP-301 | 0.98 | 54.63 | 37.8 | 6.59 |
| | | Ad-p53 | 3.51 | 49.4 | 37.35 | 9.74 |
| | | Ad-p53 + OBP-301 | 24.95 | 44.95 | 25.03 | 5.07 |
| SW620 | | Mock | 3.06 | 49.52 | 35.11 | 11.77 |
| | Day 2 | OBP-301 | 4.9 | 49.79 | 30.6 | 14.71 |
| | | Ad-p53 | 5.71 | 68.3 | 15.28 | 10.71 |
| | | Ad-p53 + OBP-301 | 7.08 | 60.91 | 20.76 | 11.25 |
| | Day 5 | OBP-301 | 5.93 | 37.18 | 40.35 | 16.54 |
| | | Ad-p53 | 4.03 | 57.7 | 24.26 | 14.01 |
| | | Ad-p53 + OBP-301 | 30.29 | 54.52 | 10.46 | 4.73 |

NOTE: H1299 cells were infected with 1 MOI of OBP-301, 5 MOI of Ad-p53, or a combination of both and harvested on days 2 and 5. SW620 cells were infected with 1 MOI of OBP-301, 50 MOI of Ad-p53, or a combination of both and harvested on days 2 and 5. Cell cycle analysis was determined by the fluorescence-activated cell sorter (FACSCalibur) flow cytometer.

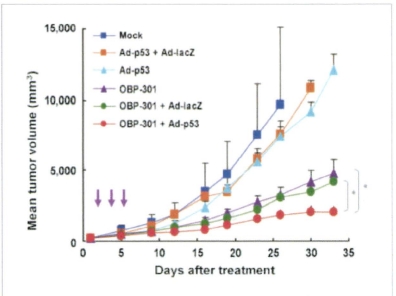


Figure 6. H1299 cells ($7.5 \times 10^6$ cells/mouse) were injected s.c. into the flank of BALB/c *nu/nu* mice and permitted to grow to 4 to 10 mm in diameter. A 50 μL solution containing Ad-p53 ($1 \times 10^9$ pfu), OBP-301 ($1 \times 10^7$ pfu), OBP-301 ($1 \times 10^7$ pfu) + Ad-p53 ($1 \times 10^8$ pfu), or Ad-lacZ ($1 \times 10^8$ pfu), Ad-p53 ($1 \times 10^8$ pfu) + Ad-lacZ ($1 \times 10^7$ pfu), or PBS was injected into the tumor for three cycles every 2 d. The perpendicular diameter of each tumor was measured every 3 or 4 d. Six or seven mice were used for each group. Points, mean tumor growth volume; bars, SE. *, $P < 0.05$, statistical significance (Student's *t* test). Arrows, days of treatment.

## Discussion

Resistance to apoptosis is a major cause of treatment failure in human cancers. Many combination regimens with clinically available agents are currently being used; however, there is a need for a better understanding of the molecular interaction of drugs to efficiently induce apoptosis in human cancer cells. In the present study, our goal was to determine whether dual virotherapy, which mediates telomerase-specific enhancement of exogenous wild-type p53 gene expression, was effective for inducing apoptosis. We found that Ad-p53 and OBP-301, with different mechanisms of action, could be more effective in the growth of human cancer cells than Ad-p53 or OBP-301 alone *in vitro* as well as *in vivo*. Moreover, our data suggest that p53-induced p21 induction was inhibited in the presence of OBP-301 infection, which might in turn sensitize tumor cells to apoptosis by blocking cell cycle arrest.

Virotherapy for p53 gene transfer by Ad-p53 (Advexin) is currently in clinical trials as a cancer therapeutic (24). Overexpression of p53 gene caused preferential cancer cell–killing, although this was less toxic to normal cells, which means that p53 gene therapy itself is a cancer-targeting therapy; however, the low transduction rate and the narrow spread of Ad-p53 limits the anticancer effect *in vivo*. The major problem for p53 therapy with replication-defective adenovirus vector is incomplete transduction of target cancer cells. Therefore, cancer cells beyond transduced cells will escape the antitumor effect. To overcome the low transduction rate of replication-defective adenoviral vectors, an increment in the dose would be the simple resolution; however, a higher dose of Ad-p53 might not always contribute to the improvement of transduction efficacy and could potentially cause side effects. In this study, even the low dose of Ad-p53, administration of which solely was not enough to induce apoptosis, enabled an increase anticancer effect in combination with OBP-301 by replicating selectively in tumor cells. OBP-301 was genetically designed to replicate specifically in tumor cells, causing specific "oncolysis"(13, 15, 16), thereby increasing the effective treatment radius in tumors. This combination might contribute to the mitigation of unfavorable effects. OBP-301 is currently being evaluated in phase I trials for clinical safety as of the writing of this article.

Virotherapy with adenovirus Onyx-015, the first oncolytic virus, has been evaluated in clinical trials, and showed that administration of oncolytic adenovirus via intratumor, intraperitoneum, or intravenous methods was well tolerated (25); however, the efficacy of Onyx-015 as a single agent is also limited, possibly because of inefficient cell lysis and release of their progeny, which may be defective in cancer cells. Our strategy is aiming not only to enhance the antitumor activity of Ad-p53 by OBP-301, but also to augment the oncolytic activity of OBP-301 in combination with Ad-p53. Oncolysis is due to cytopathic effects intrinsic to the adenovirus. Adenovirus must be able to induce cell death in infected cells for the virus to generate a cytopathic effect and be released from the cell. Hall et al. showed that wild-type p53 enhances the ability of adenoviruses to induce cell death, whereas the loss of functional p53 in cancer cells resulted in a defect in adenovirus-induced cytopathic effects (26). Thus, functional p53 is required for a productive adenovirus infection. Consistent with their report, our strategy to compensate or overexpress functional wild-type p53 must be conducive to efficient adenovirus replication, which leads to effective oncolysis by OBP-301.

The efficacy of combination therapy with conventional gene therapy using replication-deficient adenovirus plus virotherapy has been reported previously (27, 28). Combined with tumor-specific replication-selective adenovirus, replication-deficient adenoviruses were able to replicate and spread to surrounding tumor cells. Antitumor activity was increased compared with gene therapy alone or virotherapy alone in agreement with our study. In our previous study, co-infection with a replication-deficient adenovirus expressing the green fluorescent protein (*GFP*) gene and OBP-301 was able to specifically visualize human lung cancer cells in an orthotopic murine model (14). Although the study showed the diagnostic application of combinative use of replication deficient adenoviral vector and OBP-301, the specific replication of coinfected adenovirus in tumor was visually evidenced. The current study applied this principle to therapeutic purpose. When Ad-p53 was used together with OBP-301, the total amount of the viruses might be higher than that of OBP-301 alone that shows the equivalent efficacy; the dose of replicative OBP-301, however, should be reduced as much as possible from the viewpoint of safety.

Indeed, the pharmacodynamic data in a phase I clinical trial of OBP-301 showed the transient systemic dissemination of OBP-301 following intratumoral injection (29).

Another interesting finding in the current study is that OBP-301 infection apparently inhibited exogenous p53-mediated expression of p21, which is a key player in arresting cells in the $G_1$ phase. This suggests that OBP-301 infection might be an important requirement for rendering tumor cells sensitive to apoptosis rather than cell cycle arrest. Indeed, it has been reported that the adenovirus E1A protein could enhance the sensitivity of tumor cells to chemotherapeutic agents by promoting apoptosis (30). This is primarily because of the ability of E1A to interact with p21 and thereby inactivate it, which in turn, leads to apoptosis. Further mechanisms of this interaction are now under investigation.

Our strategies aim to enhance the efficiency and specificity of viral agents through incorporation of tumor-targeting mechanisms via therapeutic gene and transcriptional regulation. Although this study examined the combinative use of two viral agents, oncolytic adenoviruses carrying therapeutic genes in the E1 or E3 region have also been reported (31, 32). Gene therapy and oncolytic virotherapy, however, do not always work effectively in combination (33). In case the expression level of therapeutic genes needs to be titrated, therapeutic genes might work better when separated from oncolytic virus. In addition, both p53 therapy and OBP-301 oncolytic therapy are currently being tested clinically. Once they are approved for clinical use, this study would provide realistic therapeutic applications as a preclinical study in the future.

In conclusion, our data showed that combination therapy of Ad-p53 and OBP-301 efficiently inhibited human cancer cell growth *in vitro* and *in vivo*, and that this approach has important implications for the treatment of human cancers.

## Disclosure of Potential Conflicts of Interest

Y. Urata: employee of Oncolys BioPharma, Inc. T. Fujiwara: consultant to Oncolys BioPharma, Inc. No other potential conflicts of interest were disclosed.

## Acknowledgments

We thank Daiju Ichimaru and Hitoshi Kawamura for their helpful discussions. We also thank Tomoko Sueishi for her excellent technical support.

## Grant Support

Grants-in-Aid from the Ministry of Education, Science, and Culture, Japan (T. Fujiwara) and the Ministry of Health, Labour and Welfare, Japan (T. Fujiwara).

The costs of publication of this article were defrayed in part by the payment of page charges. This article must therefore be hereby marked *advertisement* in accordance with 18 U.S.C. Section 1734 solely to indicate this fact.

Received 06/19/2009; revised 03/26/2010; accepted 04/01/2010; published OnlineFirst 05/25/2010.

## References

1. Grem JL. Biochemical modulation of 5-FU in systemic treatment of advanced colorectal cancer. Oncology (Williston Park) 2001;15:13–9.
2. Kumar S, Gao L, Yeagy B, Reid T. Virus combinations and chemotherapy for the treatment of human cancers. Curr Opin Mol Ther 2008;10:371–9.
3. Senzer N, Mani S, Rosemurgy A, et al. TNFerade biologic, an adenovector with a radiation-inducible promoter, carrying the human tumor necrosis factor α gene: a phase I study in patients with solid tumors. J Clin Oncol 2004;22:592–601.
4. Hollstein M, Sidransky D, Vogelstein B, Harris CC. p53 mutations in human cancers. Science 1991;253:49–53.
5. Levine AJ, Perry ME, Chang A, et al. The 1993 Walter Hubert lecture: the role of the p53 tumour-suppressor gene in tumorigenesis. Br J Cancer 1994;69:409–16.
6. Swisher SG, Roth JA, Nemunaitis J, et al. Adenovirus-mediated p53 gene transfer in advanced non-small-cell lung cancer. J Natl Cancer Inst 1999;91:763–71.
7. Nemunaitis J, Swisher SG, Timmons T, et al. Adenovirus-mediated p53 gene transfer in sequence with cisplatin to tumors of patients with non-small-cell lung cancer. J Clin Oncol 2000;18:609–22.
8. Swisher SG, Roth JA, Komaki R, et al. Induction of p53-regulated genes and tumor regression in lung cancer patients after intratumoral delivery of adenoviral p53 (INGN 201) and radiation therapy. Clin Cancer Res 2003;9:93–101.
9. Fujiwara T, Tanaka N, Kanazawa S, et al. Multicenter phase I study of repeated intratumoral delivery of adenoviral p53 in patients with advanced non-small-cell lung cancer. J Clin Oncol 2006;24:1689–99.
10. Bischoff JR, Kirn DH, Williams A, et al. An adenovirus mutant that replicates selectively in p53-deficient human tumor cells. Science 1996;274:373–6.
11. Rodriguez R, Schuur ER, Lim HY, Henderson GA, Simons JW, Henderson DR. Prostate attenuated replication competent adenovirus (ARCA) CN706: a selective cytotoxic for prostate-specific antigen-positive prostate cancer cells. Cancer Res 1997;57:2559–63.
12. Kim D, Martuza RL, Zwiebel J. Replication-selective virotherapy for cancer: biological principles, risk management and future directions. Nat Med 2001;7:781–7.
13. Kawashima T, Kagawa S, Kobayashi N, et al. Telomerase-specific replication-selective virotherapy for human cancer. Clin Cancer Res 2004;10:285–92.
14. Umeoka T, Kawashima T, Kagawa S, et al. Visualization of intrathoracically disseminated solid tumors in mice with optical imaging by telomerase-specific amplification of a transferred green fluorescent protein gene. Cancer Res 2004;64:6259–65.
15. Taki M, Kagawa S, Nishizaki M, et al. Enhanced oncolysis by a tropism-modified telomerase-specific replication-selective adenoviral agent OBP-405 ('Telomelysin-RGD'). Oncogene 2005;24:3130–40.
16. Fujiwara T, Kagawa S, Kishimoto H, et al. Enhanced antitumor efficacy of telomerase-selective oncolytic adenoviral agent OBP-401 with docetaxel: preclinical evaluation of chemovirotherapy. Int J Cancer 2006;119:432–40.
17. Kishimoto H, Kojima T, Watanabe Y, et al. *In vivo* imaging of lymph node metastasis with telomerase-specific replication-selective adenovirus. Nat Med 2006;12:1213–9.
18. Blackburn EH. Structure and function of telomeres. Nature 1991;350:569–73.
19. Kim NW, Piatyszek MA, Prowse KR, et al. Specific association of

human telomerase activity with immortal cells and cancer. Science 1994;266:2011–5.
20. Shay JW, Wright WE. Telomerase activity in human cancer. Curr Opin Oncol 1996;8:66–71.
21. Nakayama J, Tahara H, Tahara E, et al. Telomerase activation by hTRT in human normal fibroblasts and hepatocellular carcinomas. Nat Genet 1998;18:65–8.
22. Fujiwara T, Tanaka N, Numunaitis JJ, et al. Phase I trial of intratumoral administration of OBP-301, a novel telomerase-specific oncolytic virus, in patients with advanced solid cancer: evaluation of biodistribution and immune response. J Clin Oncol 2008;26:3572.
23. Ohtani S, Kagawa S, Tango Y, et al. Quantitative analysis of p53-targeted gene expression and visualization of p53 transcriptional activity following intratumoral administration of adenoviral p53 *in vivo*. Mol Cancer Ther 2004;3:93–100.
24. Roth JA. Adenovirus p53 gene therapy. Expert Opin Biol Ther 2006; 6:55–61.
25. Kim D. Oncolytic virotherapy for cancer with the adenovirus dl1520 (Onyx-015): results of phase I and II trials. Expert Opin Biol Ther 2001;1:525–38.
26. Hall AR, Dix BR, O'Carroll SJ, Braithwaite AW. p53-dependent cell death/apoptosis is required for a productive adenovirus infection. Nat Med 1998;4:1068–72.
27. Lee CT, Lee YJ, Kwon SY, et al. *In vivo* imaging of adenovirus transduction and enhanced therapeutic efficacy of combination therapy with conditionally replicating adenovirus and adenovirus-p27. Cancer Res 2006;66:372–7.
28. Li X, Raikwar SP, Liu YH, et al. Combination therapy of androgen-independent prostate cancer using a prostate restricted replicative adenovirus and a replication-defective adenovirus encoding human endostatin-angiostatin fusion gene. Mol Cancer Ther 2006;5:676–84.
29. Nemunaitis J, Tong AW, Nemunaitis M, et al. A phase I study of telomerase-specific replication competent oncolytic adenovirus (telomelysin) for various solid tumors. Mol Ther 2010;18: 429–34.
30. Chattopadhyay D, Ghosh MK, Mal A, Harter ML. Inactivation of p21 by E1A leads to the induction of apoptosis in DNA-damaged cells. J Virol 2001;75:9844–56.
31. Haviv YS, Takayama K, Glasgow JN, et al. A model system for the design of armed replicating adenoviruses using p53 as a candidate transgene. Mol Cancer Ther 2002;1:321–8.
32. Nanda D, Vogels R, Havenga M, Avezaat CJ, Bout A, Smitt PS. Treatment of malignant gliomas with a replicating adenoviral vector expressing herpes simplex virus-thymidine kinase. Cancer Res 2001; 61:8743–50.
33. Hioki M, Kagawa S, Fujiwara T, et al. Combination of oncolytic adenovirotherapy and Bax gene therapy in human cancer xenografted models. Potential merits and hurdles for combination therapy. Int J Cancer 2008;122:2628–33.

Cancer Research

# Telomerase-Dependent Oncolytic Adenovirus Sensitizes Human Cancer Cells to Ionizing Radiation via Inhibition of DNA Repair Machinery

Shinji Kuroda[1], Toshiya Fujiwara[1], Yasuhiro Shirakawa[1], Yasumoto Yamasaki[1], Shuya Yano[1], Futoshi Uno[1], Hiroshi Tazawa[2], Yuuri Hashimoto[1], Yuichi Watanabe[1,3], Kazuhiro Noma[1], Yasuo Urata[3], Shunsuke Kagawa[1], and Toshiyoshi Fujiwara[1,2]

## Abstract

The inability to repair DNA double-strand breaks (DSB) leads to radiosensitization, such that ionizing radiation combined with molecular inhibition of cellular DSB processing may greatly affect treatment of human cancer. As a variety of viral products interact with the DNA repair machinery, oncolytic virotherapy may improve the therapeutic window of conventional radiotherapy. Here, we describe the mechanistic basis for synergy of irradiation and OBP-301 (Telomelysin), an attenuated type-5 adenovirus with oncolytic potency that contains the human telomerase reverse transcriptase promoter to regulate viral replication. OBP-301 infection led to E1B55kDa viral protein expression that degraded the complex formed by Mre11, Rad50, and NBS1, which senses DSBs. Subsequently, the phosphorylation of cellular ataxia-telangiectasia mutated protein was inhibited, disrupting the signaling pathway controlling DNA repair. Thus, tumor cells infected with OBP-301 could be rendered sensitive to ionizing radiation. Moreover, by using noninvasive whole-body imaging, we showed that intratumoral injection of OBP-301 followed by regional irradiation induces a substantial antitumor effect, resulting from tumor cell–specific radiosensitization, in an orthotopic human esophageal cancer xenograft model. These results illustrate the potential of combining oncolytic virotherapy and ionizing radiation as a promising strategy in the management of human cancer. *Cancer Res; 70(22); 9339–48. ©2010 AACR.*

## Introduction

Current treatment strategies for advanced cancer include surgical resection, radiation, and cytotoxic chemotherapy. Preoperative or postoperative chemoradiation may improve local control and the survival of advanced cancer patients by minimizing the risk of dissemination during the surgical procedure, increasing the complete resection rate, and eradicating microscopic residual tumor cells that are not surgically removed. The lack of restricted selectivity for tumor cells is the primary limitation of radiotherapy, despite improved technologies such as stereotactic and hyperfractionated radiotherapy. Although radiotherapy is generally considered to be less invasive, the maximum doses and treatment fields are limited to avoid the influence on the surrounding normal tissues. Therefore, to improve the therapeutic index of radiotherapy while maintaining a tolerance of normal tissue toxicity, there is a need for agents that effectively lower the threshold for radiation-induced tumor cell death; the safety and efficacy of some candidates are already being explored in clinical trials (1–3).

Ionizing radiation primarily targets DNA molecules and induces double-strand breaks (DSB; ref. 4). Radiosensitization can result from a therapeutic increase in DNA DSBs or inhibition of their repair. Ataxia-telangiectasia mutated (ATM) protein is an important signal transducer of the DNA damage response, which contains DNA repair and cell cycle checkpoints, and activation of ATM by autophosphorylation occurs in response to exposed DNA DSBs (5). Cells mutated in the ATM gene have defects in cell cycle checkpoints and DNA repair and are hypersensitive to DSBs (6, 7); thus, agents that inhibit the ATM pathway can be useful radiosensitizers (8). The Mre11, Rad50, and NBS1 (MRN) complex is quickly stimulated by DSBs and directly activates ATM (9, 10). Defects in the MRN complex lead to genomic instability, telomere shortening, and hypersensitivity to DNA damage (11).

We reported previously that telomerase-specific, replication-selective adenovirus (Telomelysin, OBP-301), in which the human telomerase reverse transcriptase (hTERT) promoter element drives the expression of *E1* genes, induced selective

**Authors' Affiliations:** [1]Department of Gastroenterological Surgery, Okayama University Graduate School of Medicine, Dentistry and Pharmaceutical Sciences; [2]Center for Gene and Cell Therapy, Okayama University Hospital, Okayama, Japan; and [3]Oncolys BioPharma, Inc., Tokyo, Japan

**Note:** Supplementary data for this article are available at Cancer Research Online (http://cancerres.aacrjournals.org/).

**Corresponding Author:** Toshiyoshi Fujiwara, Department of Gastroenterological Surgery, Okayama University Graduate School of Medicine, Dentistry and Pharmaceutical Sciences, 2-5-1 Shikata-cho, Kita-ku, Okayama 700-8558, Japan. Phone: 81-86-235-7257; Fax: 81-86-221-8775; E-mail: toshi_f@md.okayama-u.ac.jp.

**doi:** 10.1158/0008-5472.CAN-10-2333

E1 expression, and efficiently killed human cancer cells but not normal human somatic cells (12–15). Adenoviral E1B55kDa protein, a gene product in the adenoviral early region, inhibits the functions of p53 and the MRN complex by cooperating with adenoviral E4orf6 protein, leading to the proteolytic degradation of these proteins (10, 16–18). In the present study, we showed the synergistic efficacy of combined treatment with ionizing radiation and OBP-301 against human cancer cells, and we clarified the E1B55kDa-mediated mechanism used by OBP-301 to inhibit DNA repair.

## Materials and Methods

### Cell lines and cell cultures

The human non–small-cell lung cancer cell line A549 was propagated in DMEM containing Nutrient Mixture (Ham's F-12) and supplemented with 10% FCS. The human esophageal squamous cell carcinoma cell line TE8 was cultured in RPMI 1640 supplemented with 10% FCS. The human esophageal adenocarcinoma cell line SEG1 was cultured in DMEM supplemented with 10% FCS. TE8 cells transfected with the firefly luciferase plasmid vector (TE8-Luc) were maintained in medium containing 0.2 mg/mL Geneticin (G418).

### Adenovirus

The recombinant, replication-selective, tumor-specific adenovirus vector OBP-301 (Telomelysin), in which the hTERT promoter element drives the expression of *E1A* and *E1B* genes linked with an internal ribosome entry site, was previously characterized (12–15). The wild-type adenovirus type 5 (Ad-wt) and the E1B55kDa-defective adenovirus mutant dl1520 (Onyx-015) were also used (19).

### Cell viability assay

A549, TE8, and SEG1 cells were infected with OBP-301 at the indicated multiplicities of infection (MOI) and then irradiated at the indicated dosages by using an MBR-1520R device (Hitachi Medical Co.). Cell viability was determined 5 days after irradiation with a Cell Proliferation Kit II (Roche Molecular Biochemicals), according to the manufacturer's protocol. Synergy between radiation and OBP-301 was analyzed with the CalcuSyn software (BioSoft), and the computation of the combination index was based on the methods of Chou and Talalay (20).

### Flow cytometry

Cells were incubated for 20 minutes on ice in Cytofix/Cytoperm solution (BD Biosciences) and labeled with phycoerythrin (PE)-conjugated rabbit monoclonal active caspase-3 antibody (BD Biosciences) for 30 minutes and analyzed by FACSArray (BD Biosciences).

### Immunofluorescence staining

Cells seeded on tissue culture chamber slides were treated and then fixed with cold methanol for 30 minutes on ice. The slides were subsequently incubated with primary antibody against pATM (Rockland), Mre11, Rad50 (GeneTex), NBS1 (Novus), and E1B55kDa (kindly provided by Dr. Arnold Levine, The Institute for Advanced Study, Princeton, NJ) for 1 hour on ice. After washing twice with PBS, slides were incubated with the secondary antibody, FITC-conjugated rabbit anti-mouse IgG (Zymed Laboratories), FITC-conjugated goat anti-rabbit IgG (Vector Laboratories), or Alexa 568–conjugated goat anti-mouse IgG (Molecular Probes), for 1 hour on ice. The slides were further stained with 4′,6-diamidino-2-phenylindole, mounted by using Fluorescent Mounting Medium (Dako Cytomation), and then analyzed with an LSM510 confocal laser microscope (Zeiss).

### Western blot analysis

The primary antibodies against pATM (Cell Signaling), ATM (Novus), Mre11, Rad50, NBS1, E1B55kDa (kindly provided by Dr. Levine), γH2AX (Upstate), poly(ADP-ribose) polymerase (PARP; Cell Signaling), β-actin (Sigma), and peroxidase-linked secondary antibodies (Amersham) were used. Proteins were electrophoretically transferred to Hybond-polyvinylidene difluoride transfer membranes (GE Healthcare Life Science) and incubated with primary antibody, followed by peroxidase-linked secondary antibody. The Amersham ECL chemiluminescence system (GE Healthcare Life Science) was used to detect the peroxidase activity of the bound antibody.

### *In vivo* subcutaneous human tumor model

A549, TE8, and SEG1 cells ($2 \times 10^6$ per mouse) were injected s.c. into the flanks of 5- to 6-week-old female BALB/c *nu/nu* mice. When tumors reached ~3 to 5 mm in diameter, the mice were irradiated at a dosage of 3 Gy/tumor every 2 days (for A549) or 2 Gy/tumor every week (for TE8 and SEG1) for three cycles starting at day 0. When irradiated, mice were placed prone in custom-made holders that contain lead collimators to shield the upper half of the mice. Immediately after radiation, OBP-301 at a dose of $1 \times 10^8$ plaque-forming units (PFU)/tumor or PBS was injected into the tumor. In experiments with larger tumors, subcutaneous TE8 tumors with a diameter of 8 to 10 mm were treated with radiation at 2 Gy/tumor and intratumoral injection of OBP-301 at $1 \times 10^8$ PFU/tumor three times per week (every 2 days) for three cycles (nine times in total). The perpendicular diameter of each tumor was measured every 3 to 4 days, and tumor volume was calculated with the following formula: tumorvolume ($mm^3$) = $a \times b^2 \times 0.5$, where $a$ is the longest diameter, $b$ is the shortest diameter, and 0.5 is a constant to calculate the volume of an ellipsoid. The experimental protocol was approved by the Ethics Review Committee for Animal Experimentation of Okayama University.

### Orthotopic human esophageal cancer model

TE8-Luc cells ($2 \times 10^6$ per mouse) suspended in Matrigel were inoculated into the abdominal esophagus of 6-week-old female BALB/c *nu/nu* mice during laparotomy. Three weeks later, mice were irradiated with 2 Gy/tumor in holders that contain lead collimators to shield the head, neck, and chest of the mice. Immediately after radiation, mice were intratumorally injected with OBP-301 at $1 \times 10^8$ PFU/tumor during laparotomy, every 2 days for three cycles. To monitor tumor progression, the substrate luciferin was injected i.p. at a dose

of 150 mg/kg body weight. Images were collected in the supine position every few minutes from 10 to 30 minutes after luciferin injection with the IVIS Imaging System (Xenogen), and photons emitted from the abdominal esophagus region were quantified by using Living Image Software (Xenogen).

### Statistical analysis

All data were expressed as mean ± SD. Differences between groups were examined for statistical significance with the Student's *t* test. *P* values <0.05 were considered statistically significant.

## Results

### Radiosensitizing effect of OBP-301 *in vitro*

To examine the potential interaction between OBP-301 and ionizing radiation *in vitro*, we first evaluated their combined effect in human lung (A549) and esophageal (TE8 and SEG1) cancer cell lines. The cells received a single dose of ionizing irradiation 24 hours after either mock or OBP-301 infection, and the cell viability was assessed by 2,3-bis[2-methoxy-4-nitro-*S*-sulfophenyn]*H*-tetrazolium-5-carboxanilide inner salt (XTT) assay 5 days after irradiation. The addition of OBP-301 increased the cytotoxicity of ionizing radiation in a dose-dependent manner. The combination index showed potent, statistically significant synergy between OBP-301 and radiation in all three cell lines (Fig. 1A). In contrast, synergy was not observed in normal human lung fibroblasts (NHLF) because the viral replication of OBP-301 was attenuated in telomerase-negative normal cells (Supplementary Fig. S2A, B).

We measured the amount of apoptosis in A549 and TE8 cells that were irradiated after OBP-301 infection. The cells were infected with OBP-301 at a MOI of 1.0, irradiated with a dose of 10 Gy 24 hours after infection, and analyzed for apoptosis. OBP-301 caused a significant increase in active caspase-3–positive cells in response to ionizing irradiation (Fig. 1B). Western blot analysis showed that ionizing radiation promoted the cleavage of PARP, a caspase-3 substrate and a biochemical marker of apoptosis, with prior OBP-301 infection (Fig. 1C). Moreover, OBP-301 infection before irradiation significantly increased the number of A549 cells with apoptotic nuclear morphology (Fig. 1D and E). Thus, OBP-301 combined with ionizing radiation synergistically increased the amount of apoptosis.

### Degradation of the MRN complex by adenoviral E1B55kDa protein

To elucidate the molecular mechanism responsible for the synergy between OBP-301 and ionizing radiation, we examined the physical interaction between viral proteins and the MRN complex, which drives the DNA repair pathway as a sensor of DNA DSBs, through a series of confocal microscopy experiments. Immunofluorescence staining of A549 cells infected with OBP-301 at an MOI of 10 showed colocalization of the signals representing Mre11, NBS1, and Rad50, suggesting that these proteins exist as a complex. Moreover, there was marked overlap in the nuclear signals corresponding to adenoviral E1B55kDa and NBS1, indicating a direct interaction between the E1B55kDa protein and the MRN complex (Fig. 2A). Western blot analysis showed that the levels of Mre11, NBS1, and Rad50 protein gradually decreased after OBP-301 infection at an MOI of 10, as the E1B55kDa expression increased (Fig. 2B). The expression of the MRN complex remained unchanged in NHLF because E1B55kDa expression was absent after OBP-301 infection (Supplementary Fig. S2C).

To confirm the effect of adenoviral E1B55kDa on the MRN degradation, we compared the subcellular localization and degradation of Mre11 protein after infection with wild-type adenovirus (Ad-wt), an adenovirus mutant that lacked E1B55kDa (dl1520, Onyx-015), or OBP-301 in A549 cells. The Mre11 protein accumulated in the nucleus in a scattered pattern within 24 hours after OBP-301 or Ad-wt infection and then relocated to the perinuclear area and was degraded; however, the scattered nuclear signals of Mre11 remained largely undegraded 72 hours after dl1520 infection (Fig. 2C). We measured the proportions of the cells with each staining pattern (scattered, perinuclear, or degraded) to compare the subcellular dynamics of the Mre11 protein. OBP-301 and Ad-wt infection caused a rapid decrease in Mre11-positive cells compared with dl1520 infection (Fig. 2D and E), suggesting that the E1B55kDa protein is essential for the degradation of the MRN complex.

### Inhibition of radiation-induced DNA damage responses by OBP-301

The MRN complex functions as a DSB sensor that activates the ATM-dependent signaling pathway, which coordinates cell cycle arrest with DNA repair. To further investigate the relationship between E1B55kDa and ATM activation, we examined the effect of OBP-301 infection on the radiation-induced phosphorylation of ATM (pATM) in A549 cells. Immunofluorescence analysis revealed spot signals of pATM throughout the nuclei 30 minutes after ionizing radiation; however, OBP-301 or Ad-wt infection (10 MOI) 24 hours before irradiation blocked the formation of pATM foci (Fig. 3A). Pretreatment with OBP-301 significantly reduced the number of pATM-positive cells compared with pretreatment with dl1520 lacking E1B55kDa (Fig. 3B). Western blot analysis also showed that ionizing radiation induced the phosphorylation of ATM, whereas expression of E1B55kDa by OBP-301 infection led to the degradation of the MRN complex, which was accompanied by a greatly reduced level of pATM (Fig. 3C). Following dl1520 infection, ATM phosphorylation was seen in the absence of E1B55kDa expression and MRN degradation.

We also investigated whether OBP-301 infection could abrogate the DNA repair process by using γH2AX, which is a sensitive indicator of DSBs. Ionizing radiation induced γH2AX expression as early as 30 minutes after treatment in both mock- and OBP-301–infected A549 cells. The levels of γH2AX protein gradually decreased as the DNA DSBs were repaired in mock-infected cells, but remained elevated in cells infected with OBP-301 24 hours before irradiation (Fig. 3D). Densitometric quantification revealed that the relative density of γH2AX/β-actin at 3 hours after irradiation decreased by 64% without prior OBP-301 infection, but decreased by only

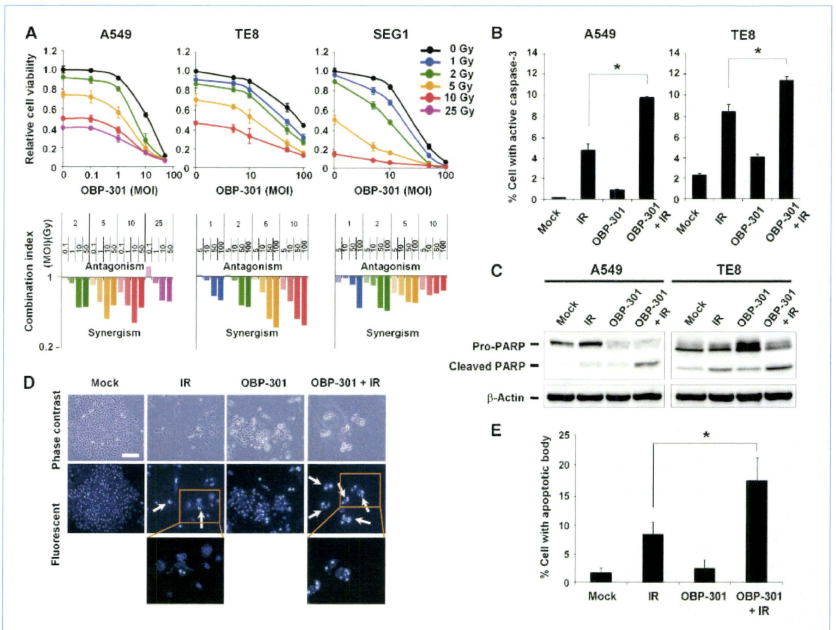


Figure 1. Radiosensitizing effect of OBP-301 on human cancer cells *in vitro*. A, cells were irradiated with the indicated doses 24 h after infection with OBP-301 at the indicated MOIs, and cell viability was assessed by XTT assay 5 d after irradiation. Top panels, percentages of viable cells relative to mock-treated cells. Error bars indicate 95% confidence intervals for triplicate data points. Bottom panels, the combination index was calculated with the CalcuSyn software. Synergy and antagonism were defined as interaction indices of <1 and >1, respectively. B to E, induction of apoptotic cell death by OBP-301 plus ionizing radiation. A549 and TE8 cells were infected with OBP-301 at an MOI of 1, irradiated with 10 Gy 24 h after infection, and then collected 5 d after irradiation. B, flow cytometric analysis for active caspase-3 expression. Cells were stained with PE-conjugated rabbit monoclonal active caspase-3 antibody and analyzed by FACS. *, $P < 0.01$. C, Western blot analysis for the cleavage of PARP. Blots were probed with anti-PARP antibody and visualized by using an ECL detection system. D, visualization of apoptotic nuclei. Treated A549 cells were stained with Hoechst 33342 and analyzed for DNA fragmentation by fluorescent microscopy. White arrows indicate cells with apoptotic bodies. The bottom panels are the magnified views of the boxed region in the middle panels. IR, ionizing radiation. E, the percentage of apoptotic cells was calculated by counting the number of cells with apoptotic bodies per 100 cells in six random fields in each group.

19% with OBP-301 infection compared with the levels at 30 minutes postirradiation (Fig. 3E). These results indicate that OBP-301 infection interrupts the cellular DNA repair mechanism induced by ionizing radiation.

### Synergistic antitumor activity of OBP-301 plus radiation in human tumor xenografts

We next assessed the therapeutic efficacy of OBP-301 in combination with ionizing radiation against A549, TE8, and SEG1 cells *in vivo*. To determine the treatment schedule, we examined whether radiation could modify adenoviral infectivity and replication in human cancer cells. OBP-301 infection following ionizing radiation showed synergistic antitumor effects *in vitro* (Supplementary Fig. S3) due to an increased expression density of coxsackievirus and adenovirus receptor, which resulted in enhanced adenoviral uptake in human cancer cells (Supplementary Figs. S4 to S6). We also confirmed that ionizing radiation does not interfere with OBP-301 replication (Supplementary Fig. S7).

Based on these preliminary results, we chose a therapy regimen with three cycles of regional radiation followed immediately by intratumoral administration of OBP-301. Mice bearing A549, TE8, and SEG1 subcutaneous tumors that were 3 to 5 mm in diameter received 3 Gy (for A549) or 2 Gy (for TE8 and SEG1) local irradiation followed by the intratumoral injection of either $1 \times 10^8$ PFU of OBP-301 or PBS every 2 days (for A549) or 7 days (for TE8 and SEG1) for three cycles. Intratumoral administration of OBP-301 or radiation